How to cite: Angew. Chem. Int. Ed. 2023, 62, e202306005
doi.org/10.1002/anie.202306005

Perovskites Hot Paper

Cesium Methylammonium Lead Iodide ($Cs_xMA_{1-x}PbI_3$) Nanocrystals with Wide Range Cation Composition Tuning and Enhanced Thermal Stability of the Perovskite Phase

Yangning Zhang, Omar F. Aly, Anastacia De Gorostiza, Thana Shuga Aldeen, Allison J. Segapeli, and Brian A. Korgel[*]

Abstract: Cesium methylammonium lead iodide ($Cs_xMA_{1-x}PbI_3$) nanocrystals were obtained with a wide range of A-site Cs-MA compositions by post-synthetic, room temperature cation exchange between $CsPbI_3$ nanocrystals and $MAPbI_3$ nanocrystals. The alloyed $Cs_xMA_{1-x}PbI_3$ nanocrystals retain their photoactive perovskite phase with incorporated Cs content, x, as high as 0.74 and the expected composition-tunable photoluminescence (PL). Excess methylammonium oleate from the reaction mixture in the $MAPbI_3$ nanocrystal dispersions was necessary to obtain fast Cs-MA cation exchange. The phase transformation and degradation kinetics of films of $Cs_xMA_{1-x}PbI_3$ nanocrystals were measured and modeled using an Avrami expression. The transformation kinetics were significantly slower than those of the parent $CsPbI_3$ and $MAPbI_3$ nanocrystals, with Avrami rate constants, k, at least an order of magnitude smaller. These results affirm that A-site cation alloying is a promising strategy for stabilizing iodide-based perovskites.

Introduction

Lead halide perovskite nanocrystals exhibit a range of useful optical and optoelectronic properties, including size- and composition-tunable band gap, high photoluminescence (PL) quantum yield, and defect tolerance.[1–5] Lead iodide perovskite (LIP) nanocrystals in particular are promising for solar cells and red light-emitting diodes (LEDs) because of their red-to-near infrared (NIR) wavelength optical response.[4,6–8]

Compared to their bromide counterparts, LIP nanocrystals are more challenging to synthesize and stabilize. Methylammonium lead iodidie ($MAPbI_3$) nanocrystals chemically decompose to PbI_2 and volatile degradation products when heated to relatively modest temperatures (60–90 C), due to the high volatility of the organic MA^+ ($CH_3NH_3^+$) cation.[9] $CsPbI_3$ nanocrystals are more chemically stable than $MAPbI_3$, but the equilibrium phase below ≈300 C is the optically inactive (yellow) non-perovskite orthorhombic δ-phase.[10a] It turns out that $CsPbI_3$ nanocrystals can be synthesized in the perovskite (γ-orthorhombic) phase due to capping ligand stabilization, but the nanocrystals are still highly susceptible to degradation to the δ-phase in the presence of humidity, especially at elevated temperature (190–200 C).[10b]

One approach to improve the stability of LIP is A-site compositional alloying.[11] Cs incorporation has significantly improved the stability of $MAPbI_3$ films, enabling the fabrication of efficient and stable solar cells.[12,13] Cs incorporation into $MAPbI_3$ nanocrystals has also been explored, but only a limited range of Cs:MA ratios have been obtained synthetically. For example, Navas et al.[14] has made $Cs_xMA_{1-x}PbI_3$ nanocrystals with x up to 0.2 by dropwise addition of a precursor mixture of MAI, CsI, and PbI_2 in DMF and capping ligands into a eutectic mixture of diphenyl oxide and biphenyl. Higher Cs incorporation could not be achieved. When higher Cs:MA ratios were used in the reaction, only a mixture of $Cs_{0.2}MA_{0.8}PbI_3$ and non-perovskite δ-phase $CsPbI_3$ nanocrystals were obtained.

Other LIP nanocrystals have been obtained with a wider range of mixed cation composition using cation exchange.[8,15,16] For example, cesium formamidinium lead iodide ($Cs_xFA_{1-x}PbI_3$) with over the full range of Cs:FA compositions were produced by mixing solvent dispersions of $CsPbI_3$ and $FAPbI_3$ nanocrystals at room temperature.[8] The low energy barrier to A-site cation migration and vacancy formation in the perovskite lattices enables efficient cation exchange.[17] Nonetheless, the kinetics of A-site cation exchange reactions have varied significantly in the literature–taking only a few minutes in some cases, to several hours in others. The reason for this is not well understood, but it relates to the details of the ligand chemistry.[8,16,18] So far, there have not been any published reports of $Cs_xMA_{1-x}PbI_3$ nanocrystals by cation exchange, which is most likely due to (1) difficulties in obtaining phase-pure and uniform $CsPbI_3$ and $MAPbI_3$ nanocrystals as starting materials and (2) the need for a favorable ligand environment for the cation exchange reaction.

[*] Dr. Y. Zhang, O. F. Aly, A. De Gorostiza, T. Shuga Aldeen, A. J. Segapeli, Prof. Dr. B. A. Korgel
McKetta Department of Chemical Engineering and Texas Materials Institute, The University of Texas at Austin
Austin, TX 78712-1062 (USA)
E-mail: korgel@che.utexas.edu
T. Shuga Aldeen
Department of Physics, Faculty of Science, Sana'a University
Sanaa, Yemen

Here, we report the synthesis of perovskite-phase $Cs_xMA_{1-x}PbI_3$ nanocrystals with a wide range of cation composition. These nanocrystals are obtained by cation exchange using phase-pure, relatively uniform $CsPbI_3$ and $MAPbI_3$ nanocrystals. The $Cs_xMA_{1-x}PbI_3$ nanocrystals exhibit composition-dependent absorbance and PL emission spectra. Cs content as high as $x=0.74$ was obtained without any □-phase $CsPbI_3$ byproduct. We found that the Cs-MA cation exchange kinetics are significantly accelerated when the parent $CsPbI_3$ and $MAPbI_3$ nanocrystal dispersions still contain unreacted methylammonium oleate. When mixtures of well-purified nanocrystal dispersions are combined, cation exchange is very slow, taking days to complete. Simple addition of oleic acid and/or oleylamine to the cation exchange mixture containing highly purified parent nanocrystals only results in degradation of the materials and loss of PL. Finally, we observed that the $Cs_xMA_{1-x}PbI_3$ nanocrystals were significantly more stable than the $CsPbI_3$ and $MAPbI_3$ nanocrystals.

Figure 1 shows UV/Vis absorbance and photoluminescence (PL) emission spectra of the $CsPbI_3$ and $MAPbI_3$ nanocrystals used for cation exchange.[9,10b] The $CsPbI_3$ nanocrystals exhibit an excitonic absorption peak at 647 nm (1.92 eV) and the absorption edge of the $MAPbI_3$ nanocrystals was observed at 750 nm. Both sets of nanocrystals fluoresce with PL peaks at 665 nm (1.86 eV) and 732 nm (1.69 eV), respectively, as expected for these materials. Figure 1 also shows absorbance and PL spectra for $Cs_xMA_{1-x}PbI_3$ nanocrystals obtained by cation exchange. Nanocrystals with a wide range of composition, x, could be obtained in less than 1 h by mixing $CsPbI_3$ and $MAPbI_3$ nanocrystals dispersed in hexane at room temperature with the desired [Cs:MA] molar ratio. The compositions of the nanocrystals determined from the PL peak positions in Figure 1b—assuming a linear relation between band gap and cation composition[8]—matched values of $x=0.35$, 0.55, and 0.74, which are close to those expected based on the Cs:MA mole ratios used in the cation exchange reactions of 1:2, 1:1 and 2:1, respectively. (See detailed calculations of cation compositions in Supporting Information, Figure S1 and Table S1.) The compositions of $Cs_xMA_{1-x}PbI_3$ nanocrystals were further confirmed by quantitative elemental analysis from X-ray photoelectron spectroscopy (XPS, see Supporting Information, Figure S2). The Cs to Pb ratios determined from XPS (0.33, 0.55, and 0.68) are very close to the compositions estimated from the PL peak positions of $Cs_{0.35}MA_{0.65}PbI_3$, $Cs_{0.55}MA_{0.45}PbI_3$, and $Cs_{0.74}MA_{0.26}PbI_3$.

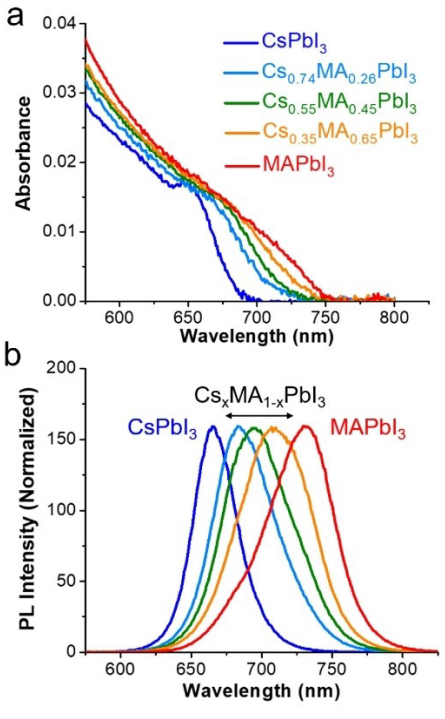

Transmission electron microscopy (TEM) images of nanocrystals of $CsPbI_3$, $MAPbI_3$, and a cation exchange product, $Cs_{0.55}MA_{0.45}PbI_3$, are shown in Figures 2a–d. The $CsPbI_3$ nanocrystals have a cube shape and are relatively uniform with average edge lengths of 6.8 ± 0.8 nm. The $MAPbI_3$ nanocrystals are cuboidal in shape and slightly less uniform, with average edge lengths of 11.1 ± 3.9 nm. The $Cs_{0.55}MA_{0.45}PbI_3$ nanocrystals have a cuboidal shape as well, most resembling the $MAPbI_3$ nanocrystals, with a slightly larger average edge length of 12.6 ± 3.7 nm. (Histograms are provided as Figure S3 as Supporting Information.)

Figure 2e shows powder XRD for the $CsPbI_3$, $MAPbI_3$ and $Cs_{0.55}MA_{0.45}PbI_3$ nanocrystals. For the parent nanocrystals, the diffraction patterns match those of black □-orthorhombic perovskite $CsPbI_3$ (*Pbnm*, $a=8.646$ Å, $b=8.818$ Å, $c=12.520$ Å) and □-tetragonal perovskite $MAPbI_3$ (*I4cm*, $a=b=8.849$ Å, $c=12.642$ Å).[9,10b,19] The diffraction pattern obtained from the cation exchange product nanocrystals of $Cs_{0.55}MA_{0.45}PbI_3$ most closely resembles □-orthorhombic $CsPbI_3$, without any evidence of non-perovskite □-orthorhombic $CsPbI_3$ (*Pnma*, $a=10.458$ Å, $b=4.802$ Å, $c=17.776$ Å) or hexagonal PbI_2 (*P-3m1*, $a=b=4.56$ Å, $c=6.98$ Å, □=□=90°, □=120°). The lattice fringes in the $Cs_{0.55}MA_{0.45}PbI_3$ nanocrystal imaged by high-resolution TEM in Figure 2d are separated by 3.1 Å, which corresponds to (2–20) *d*-spacing in the □-orthorhombic lattice. Compositional mapping by energy-dispersive X-ray spectroscopy (EDS) also showed that the nanocrystal composition is homogeneous throughout the sample and phase-pure. (See for example, data for $Cs_{0.55}MA_{0.45}PbI_3$ nanocrystals in Supporting Information, Figures S4–S5 and Table S3). Also, as shown in Figure 2f, there is a slight shifting of the (004)/(220) diffraction peak at 2□=26–30° with composition, as expected in the case of A-site alloying with species of different size. Cs^+ (ionic radius 1.80 Å) is significantly smaller than MA^+ (ionic radius 2.17 Å).[20]

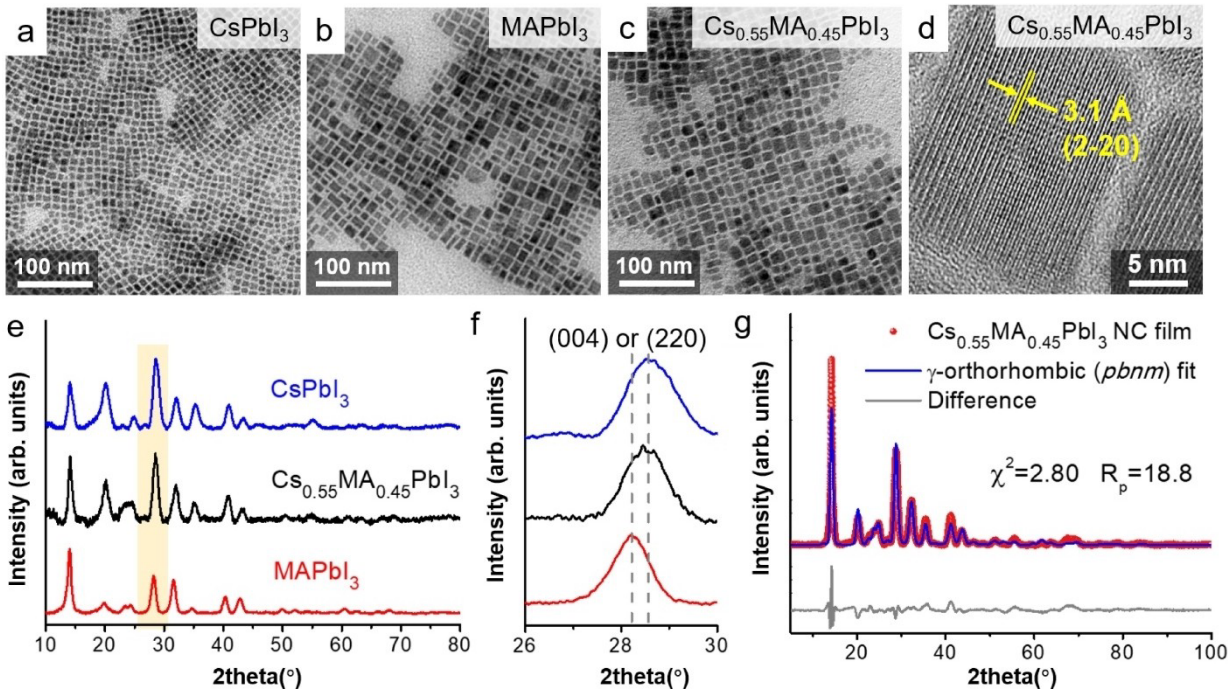

We also ruled out the possibility that the $Cs_{0.55}MA_{0.45}PbI_3$ nanocrystals could have □-tetragonal crystal structure like $MAPbI_3$–as opposed to □-orthorhombic $CsPbI_3$ (Supporting Information, Figure S6a). The diffraction peaks at 2□ = 22–28 are characteristic of the □-orthorhombic phase, as these peaks do not appear in diffraction patterns from either □-tetragonal or □-cubic phases. Quantitative analysis of the crystal structure by Rietveld refinement using □-orthorhombic models (Figure 2g) provided better goodness-of-fit metrics for the *pbnm* space group than the *pnam* space group (see Supporting Information, Figure S6b and Table S4 for detailed structural information determined from fitting). A preferred crystal orientation was also observed, with (002)/(110) planes lying parallel to the substrate in $Cs_{0.55}MA_{0.45}PbI_3$ nanocrystal films, as evidenced by the strongest diffraction peak at 2□ = 14.3 . We observed a similar preferred orientation of (002)/(110) planes in □-$CsPbI_3$ nanocrystal films in prior work.[10b]

The purification of the parent nanocrystals greatly affected the rate of cation exchange. Figure 3 shows PL spectra for four different cation exchange reactions using 1:1 molar ratios of Cs:MA. As Cs and MA cations exchange between nanocrystals, the two distinct PL peaks at 665 nm and 732 nm disappear and merge into a new PL peak at 695 nm. In Figure 3a, the crude reaction mixtures of $CsPbI_3$ and $MAPbI_3$ nanocrystals were purified by only a single precipitation with methyl acetate and then combined with equivalent molar concentrations. Under these conditions, the cation exchange is complete within one hour. Within a few minutes of mixing, the PL of the $CsPbI_3$ nanocrystals starts to red-shift, and the PL of the $MAPbI_3$ nanocrystals begins to blue-shift. Eventually, the two distinct PL peaks merge into one broad PL peak that stops changing after the cation exchange reaction has reached equilibrium. As shown in Supporting Information, Figure S7, the relative concentrations of the $CsPbI_3$ and $MAPbI_3$ nanocrystals did not affect the exchange kinetics.

Figure 3b shows the evolution of the PL spectra when the parent $MAPbI_3$ nanocrystals had been purified with an additional precipitation step. In this case, the cation exchange kinetics are very slow. Even after 3 h, the PL peaks corresponding to the $CsPbI_3$ and $MAPbI_3$ nanocrystals remain distinct and have only slightly red- and blue-shifted. After 24 h, cation exchange does finally reach completion. These results show that there are unreacted species, ligands and/or other reaction byproducts,[21] still present in the parent nanocrystal dispersions obtained after only one precipitative wash with methyl acetate that help speed the cation exchange reaction.

We tested whether the addition of excess ligand (oleic acid (OA) and/or oleylamine (OAm)) would accelerate the cation exchange reaction. Figures 3c and d show the evolution of the PL spectra of mixtures of $CsPbI_3$ nanocrystals precipitated once and $MAPbI_3$ nanocrystals precipi-

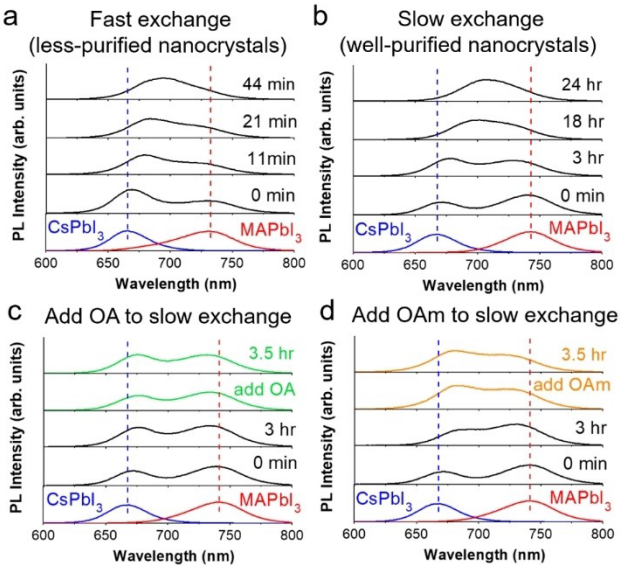

=

tated twice. The exchange reaction is very slow and even after 3 h, there was only very little shifting of the PL peaks. At this point, either OA (Figure 3c) or OAm (Figure 3d) was added to the reaction mixture in excess at a concentration of 0.05 mmol mL ^{1}. This concentration corresponds to the addition of about two additional ligand monolayers per nanocrystal to the dispersion. To put this into further context, the ligand concentration is about nine times higher than this in the crude reaction mixture. As shown in Figures 3c,d, there was still only minimal shifting of PL peak positions after 30 min of adding the excess OA or OAm. Not only did the excess OA and OAm not enhance the rate of cation exchange, the additional ligands quenched the PL of the nanocrystals and after 24 h, the samples had gone completely dark. Adding OA immediately after mixing $CsPbI_3$ and $MAPbI_3$ nanocrystals or increasing the concentration of OA to 0.10 mmol mL ^{1} still did not accelerate the cation exchange reactions (Supporting Information, Figure S8), and adding OAm initially to the nanocrystals rapidly quenched the PL of the $MAPbI_3$ nanocrystals.

To identify the species responsible for promoting fast Cs-MA cation exchange, we examined $MAPbI_3$ nanocrystals after one or two precipitation steps using nuclear magnetic resonance (NMR) spectroscopy and nuclear Overhauser effect spectroscopy (NOESY). As shown in Figure 4, OA and OAm both exhibit peaks at 5.35 ppm and 2.0 ppm, which correspond to H atoms (**8**, **9**, **10**, and **11**) near the C=C double bonds. The unique signals of OAm are the protons within the amine group (□-H) and the protons closest to the amine group (□-H), respectively.[22–25] We observed a broad peak of □-H at 3.2 ppm, indicating that OAm is interacting with the nanocrystal surface, which is further confirmed by the positive (blue) NOE cross peaks between these signals of OAm in NOESY. The small peaks at 6.1–6.4 ppm could belong to the □-H of OAm, methylamine, or their protonated species. The unique signal of OA at 2.3–2.4 ppm corresponds to the proton closest to the carboxylic group (**2**-H).[23–25] The positive (blue) NOE cross peaks between the **2**-H signal and other signals of OA suggest that OA is also bonded to the nanocrystal surface. Additional precipitation steps usually remove significant amounts of OAm and OA and, as expected, the peak intensities of □- and **2**-protons are all reduced in the more-purified sample compared with the less-purified sample.

We noticed that there was an additional peak at 3.5–3.6 ppm in the NMR spectra of the sample purified once, which was absent from the spectra of the samples purified twice. This signal corresponds to several positive cross peaks in NOESY. One of the cross interactions occurs between this signal and **2**-H of OA, but there is no observable cross interaction between this signal and □-H of OAm. Therefore, this signal should belong to a proton from OA, or from a type of oleate, like methylammonium-oleate. In the hot-injection synthesis of $MAPbI_3$ nanocrystals, methylammonium oleate is formed as an intermediate reagent to provide MA^+ ions for the formation of $MAPbI_3$.[9,21] Methylammonium oleate can also act as a surface capping ligand for $MAPbI_3$ nanocrystals.[23] In $MAPbI_3$ nanocrystals that were purified by a single precipitation with methyl acetate, there is a large amount of excess methylammonium oleate. The additional purification cycle washes away most of it, therefore its proton signal (at 3.5–3.6 ppm) is no longer visible in the NMR and NOESY spectra.

A proposed cation cross-exchange mechanism is illustrated in Scheme 1, occurring by vacancy-mediated ion diffusion and migration.[16] First, Cs^+ migrates out of the

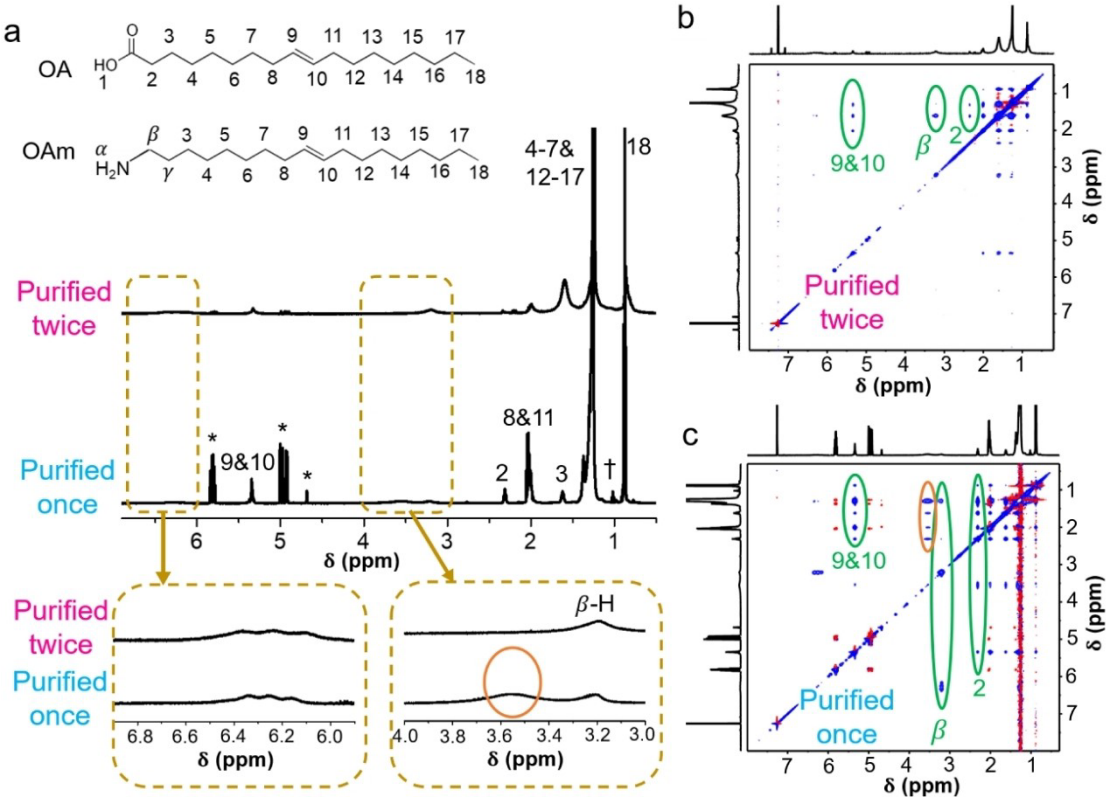

$CsPbI_3$ lattice, and MA^+ migrates out of the $MAPbI_3$ lattice, leaving behind cation vacancies. Next, Cs^+ diffuses into the $MAPbI_3$ nanocrystals to occupy the MA^+ vacancies and MA^+ diffuses into the $CsPbI_3$ nanocrystals to occupy the Cs^+ vacancies. The cation cross-exchange process reaches equilibrium when a homogeneous composition is obtained in all the $Cs_xMA_{1-x}PbI_3$ nanocrystals. When the less-purified $MAPbI_3$ nanocrystals are mixed with $CsPbI_3$ nanocrystals, the high concentration of excess methylammonium oleate provides a large concentration gradient between the free MA^+ ions in solution and the MA^+ ions in the perovskite nanocrystals. This concentration gradient drives the diffusion process of MA^+ ions toward and into $CsPbI_3$ nanocrystals and promotes the Cs-MA cation exchange reaction to reach an equilibrium. Therefore, the speed of Cs-MA cation exchange is significantly accelerated in parent nanocrystal mixtures that were less purified.

While fast cation exchange kinetics is preferred to quickly obtain mixed-cation nanocrystal compositions, in some cases, slower exchange kinetics is preferred. For example, in tandem solar cells that combine perovskite nanocrystals of different cation or anion compositions placed in adjacent layers, it is important to suppress ion exchange between nanocrystals. Strategies have been reported to suppress halide anion exchange in perovskite nanocrystals, such as introducing a protective capping layer.[26] Our study shows that cation exchange might also be significantly slowed by eliminating the presence of cation-oleate species, such as methylammonium oleate.

The thermal stability and phase transformation kinetics of the $Cs_xMA_{1-x}PbI_3$ nanocrystals were compared to the $CsPbI_3$ and $MAPbI_3$ nanocrystals. Films of nanocrystals were heated to a fixed temperature and then imaged with a camera to monitor the color change and determine the fraction of the sample that had transformed over time.[27] Our previous in situ X-ray scattering studies showed that $MAPbI_3$ nanocrystals chemically degrade at 75–90 C into PbI_2, and $CsPbI_3$ nanocrystals change from the black □-orthorhombic perovskite phase to the yellow □-orthorhombic non-perovskite phase at 190–200 C in air.[9,10b]

Films of $Cs_{0.55}MA_{0.45}PbI_3$, $CsPbI_3$ and $MAPbI_3$ nanocrystals exposed to air were rapidly heated to 210 C. This temperature is slightly above the onset temperature for the black-to-yellow phase transformation in $CsPbI_3$ nanocrystals. Figure 5a shows some characteristic images of the films as they change color from black/brown to yellow as they degrade. The area fraction of yellow material was determined by image analysis, and signifies the amount of sample degraded to the yellow phase. Figure 5b shows the evolution of the film to the yellow phase as a function of time. $CsPbI_3$

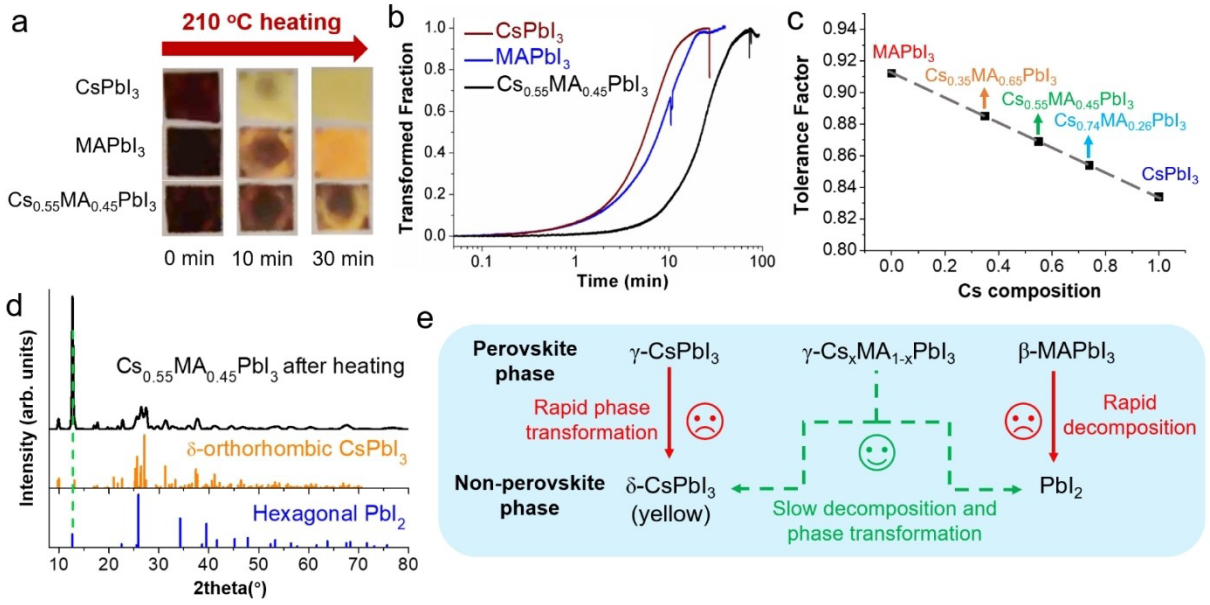

=

and $MAPbI_3$ nanocrystal films turned completely yellow in 20 min and 30–40 min respectively, while the $Cs_{0.55}MA_{0.45}PbI_3$ nanocrystals took ≈80 min to turn completely yellow.

We modeled the transformation curves in Figure 5b using the Avrami equation.[28,29] The Avrami model [Eq. (1)] has been applied to kinetic analyses of crystallization and degradation processes in bulk perovskites.[27]

$$V_c(t) = 1 \quad \exp(\quad kt^n) \tag{1}$$

In Equation (1), t is time, and $V_c(t)$ represents the transformed molar fraction of nanocrystals at time t. The rate constant k and the growth constant n can be determined by fitting the kinetic curves in Figure 5b (the fitted curves are provided in Figure S9, Supporting Information). Table 1 summarizes the fitted results for the phase transformation processes in $Cs_{0.55}MA_{0.45}PbI_3$, $CsPbI_3$ and $MAPbI_3$ nanocrystals. The rate constant k of $MAPbI_3$ is slightly smaller than $CsPbI_3$, and k of $Cs_{0.55}MA_{0.45}PbI_3$ is one order of magnitude smaller than that of $MAPbI_3$ or $CsPbI_3$. This is consistent with the much slower color change from black to yellow in $Cs_{0.55}MA_{0.45}PbI_3$ nanocrystals compared to $MAPbI_3$ and $CsPbI_3$ nanocrystals in Figure 5a. The growth constants n of all compositions fall between 1 and 2, which suggests that the crystallization and growth process is likely one to two dimensional, which is consistent with the mixed morphology of rod and platelet structures observed in scanning electron microscope (SEM) images of the $Cs_{0.55}MA_{0.45}PbI_3$ nanocrystal films that had been heated (Supporting Information, Figure S10). The enhanced stability of $Cs_xMA_{1\ x}PbI_3$ over $MAPbI_3$ can be attributed to the lattice strain due to Cs^+ incorporation. This strain locks the motion of organic MA^+ and also suppresses the migration of I , thus mitigating the degradation of hybrid organic–inorganic perovskites.[30] The improved stability of $Cs_xMA_{1\ x}PbI_3$ compared to $CsPbI_3$ can be partly explained by larger tolerance factors of $Cs_xMA_{1\ x}PbI_3$ compared to $CsPbI_3$. Figure 5c shows tolerance factors calculated for various $Cs_xMA_{1\ x}PbI_3$ compositions from the ionic radii of the A^+, Pb^{2+}, and I ions (r_A, r_{Pb}, and r_I, values provided as Supporting Information in Table S5.):

$$t = (r_A + r_I)/\sqrt{2}(r_{Pb}+r_I) \tag{2}$$

Stable metal halide perovskites have tolerance factors in the range of $0.8 \le t \le 1.0$ and the tolerance factor for $CsPbI_3$ of 0.83 lies at the bottom end of this range. The tolerance factors for $Cs_xMA_{1\ x}PbI_3$ ($x = 0.35$, 0.55, 0.74) lie in the range of 0.85–0.89, indicating that the perovskite phase stability should be higher than $CsPbI_3$. It is also possible that the H I hydrogen bonding formed when MA^+ is introduced into $CsPbI_3$ lattice helps to stabilize the 3D perovskite

structure, similar to the case of introducing MA^+ into $FAPbI_3$ (MA^+ has stronger hydrogen bonding than FA^+).[32]

We also characterized the thermal degradation products of the $Cs_{0.55}MA_{0.45}PbI_3$ nanocrystals. The XRD pattern in Figure 5d of a $Cs_{0.55}MA_{0.45}PbI_3$ nanocrystal film after thermal degradation at 210 C showed a mixture of δ-orthorhombic $CsPbI_3$ and hexagonal PbI_2 (see Supporting Information, Figure S11 for comparison of XRD before and after heating). The nanorods in the SEM image in Figure S10 are a characteristic morphology of yellow-phase $CsPbI_3$, and the nanoplatelets are characteristic of hexagonal phase PbI_2. The strongest XRD peak at $2\theta = 12.7$ indexes to the (001) planes of PbI_2, indicating a strong preferred orientation of PbI_2 (001) planes on the substrate. Furthermore, the degraded film is no longer fluorescent (see photographs of films under UV lamp in Supporting Information, Figure S12). Thermal degradation of $Cs_{0.55}MA_{0.45}PbI_3$ involves (1) phase segregation from $Cs_{0.55}MA_{0.45}PbI_3$ to $CsPbI_3$ and $MAPbI_3$,[12] (2) chemical decomposition of $MAPbI_3$ into PbI_2 and MAI (which further decomposes into volatile species such as CH_3NH_2 and HI, or CH_3I and NH_3),[9,33–35] and (3) the black-to-yellow phase transformation of $CsPbI_3$.[10b,36,37] The thermal decomposition process of $Cs_xMA_{1-x}PbI_3$ nanocrystals appears to be reversed from its formation process, with the expulsion of the MA from the $CsPbI_3$ lattice and the loss of the perovskite phase, combined with the decomposition of $MAPbI_3$.

Conclusion

We designed post-synthetic A-site cation exchange reactions and obtained $Cs_xMA_{1-x}PbI_3$ ($x = 0.35$, 0.55, and 0.74) nanocrystals by mixing $CsPbI_3$ nanocrystals and $MAPbI_3$ nanocrystals at room temperature. The Cs content of the resulting $Cs_xMA_{1-x}PbI_3$ nanocrystals reached as high as $x = 0.74$, exceeding the reported substitution limit of $x < 0.2$ in directly-synthesized $Cs_xMA_{1-x}PbI_3$ nanocrystals. The PL emission of these nanocrystals can be tuned from 665 nm to 732 nm by tuning A-site cation compositions. We found that the cation exchange kinetics were significantly enhanced by residual unreacted reagents and ligands in less-purified parent nanocrystals. NMR and NOESY analysis suggested that the key promoter for fast cation exchange reactions is likely methylammonium oleate. We also studied the structural transformation kinetics of the $Cs_xMA_{1-x}PbI_3$ nanocrystals. The $Cs_xMA_{1-x}PbI_3$ nanocrystals exhibit γ-orthorhombic perovskite crystal structure. When heated at 210 C, the perovskite to non-perovskite phase transformation in $Cs_{0.55}MA_{0.45}PbI_3$ nanocrystals is slower than in $CsPbI_3$ and $MAPbI_3$ nanocrystals. The final solid degradation products of $Cs_{0.55}MA_{0.45}PbI_3$ nanocrystals were non-perovskite phase $CsPbI_3$ and PbI_2. This work not only expands the composition range of phase-pure and red-emitting mixed A-site cation perovskite nanocrystals, but also shows that A-site compositional alloying is a promising approach to enhancing the stability of perovskite nanocrystals.

Supporting Information

The authors have cited additional references within the Supporting Information.[38]

Acknowledgements

Financial support of this work was provided by the Robert A. Welch Foundation (F-1464), the Center for a Solar Powered Future (SPF2050)—an Industry-University Cooperative Research Center (IUCRC) funded by the National Science Foundation (EEC-2052814), IUCRC on Next Generation Photovoltaics (IIP-1822206), the Center for Dynamics and Control of Materials (CDCM) Materials Research Science and Engineering Center (MRSEC) (DMR-1720595). T. S. Aldeen was funded by the Institute of International Education's Scholar Rescue Fund (IIE-SRF) and the University of Texas at Austin. We thank Garrett Blake for help acquiring NOESY data and Timothy D. Siegler for helpful discussions.

Conflict of Interest

The authors declare no conflict of interest.

Data Availability Statement

The data that support the findings of this study are available from the corresponding author upon reasonable request.

Keywords: Cation Exchange · Mixed-Cation Perovskites · Perovskite Nanocrystals · Thermal Stability

[1] L. Protesescu, S. Yakunin, M. I. Bodnarchuk, F. Krieg, R. Caputo, C. H. Hendon, R. X. Yang, A. Walsh, M. V. Kovalenko, *Nano Lett.* **2015**, *15*, 3692–3696.

[2] A. Swarnkar, A. R. Marshall, E. M. Sanehira, B. D. Chernomordik, D. T. Moore, J. A. Christians, T. Chakrabarti, J. M. Luther, *Science* **2016**, *354*, 92–95.

[3] M. A. Becker, R. Vaxenburg, G. Nedelcu, P. C. Sercel, A. Shabaev, M. J. Mehl, J. G. Michopoulos, S. G. Lambrakos, N. Bernstein, J. L. Lyons, T. Stöferle, R. F. Mahrt, M. V. Kovalenko, D. J. Norris, G. Rainò, A. L. Efros, *Nature* **2018**, *553*, 189–193.

[4] A. Dey, J. Ye, A. De, E. Debroye, S. K. Ha, E. Bladt, A. S. Kshirsagar, Z. Wang, J. Yin, Y. Wang, L. N. Quan, F. Yan, M. Gao, X. Li, J. Shamsi, T. Debnath, M. Cao, M. A. Scheel, S. Kumar, J. A. Steele, M. Gerhard, L. Chouhan, K. Xu, X. Wu, Y. Li, Y. Zhang, A. Dutta, C. Han, I. Vincon, A. L. Rogach, A. Nag, A. Samanta, B. A. Korgel, C.-J. Shih, D. R. Gamelin, D. H. Son, H. Zeng, H. Zhong, H. Sun, H. V. Demir, I. G. Scheblykin, I. Mora-Seró, J. K. Stolarczyk, J. Z. Zhang, J. Feldmann, J. Hofkens, J. M. Luther, J. Pérez-Prieto, L. Li, L. Manna, M. I. Bodnarchuk, M. V. Kovalenko, M. B. J. Roeffaers, N. Pradhan, O. F. Mohammed, O. M. Bakr, P. Yang, P. Müller-Buschbaum, P. V. Kamat, Q. Bao, Q. Zhang, R. Krahne, R. E. Galian, S. D. Stranks, S. Bals, V. Biju, W. A.

Tisdale, Y. Yan, R. L. Z. Hoye, L. Polavarapu, *ACS Nano* **2021**, *15*, 10775–10981.
[5] J. Shamsi, A. S. Urban, M. Imran, L. De Trizio, L. Manna, *Chem. Rev.* **2019**, *119*, 3296–3348.
[6] L. Protesescu, S. Yakunin, S. Kumar, J. Bär, F. Bertolotti, N. Masciocchi, A. Guagliardi, M. Grotevent, I. Shorubalko, M. I. Bodnarchuk, C. J. Shih, M. V. Kovalenko, *ACS Nano* **2017**, *11*, 3119–3134.
[7] Y. Cai, H. Wang, Y. Li, L. Wang, Y. Lv, X. Yang, R. J. Xie, *Chem. Mater.* **2019**, *31*, 881–889.
[8] A. Hazarika, Q. Zhao, E. A. Gaulding, J. A. Christians, B. Dou, A. R. Marshall, T. Moot, J. J. Berry, J. C. Johnson, J. M. Luther, *ACS Nano* **2018**, *12*, 10327–10337.
[9] Y. Zhang, C. J. Thomas, A. Guillaussier, D.-M. Smilgies, B. A. Korgel, *J. Phys. Chem. C* **2019**, *123*, 17555–17565.
[10] a) R. J. Sutton, M. R. Filip, A. A. Haghighirad, N. Sakai, B. Wenger, F. Giustino, H. J. Snaith, *ACS Energy Lett.* **2018**, *3*, 1787–1794; b) C. J. Thomas, Y. Zhang, A. Guillaussier, K. Bdeir, O. Aly, H. G. Kim, J. Noh, L. C. Reimnitz, J. Li, F. L. Deepak, D.-M. Smilgies, D. J. Milliron, B. Korgel, *Chem. Mater.* **2019**, *31*, 9750–9758.
[11] a) C. Yi, J. Luo, S. Meloni, A. Boziki, N. Ashari-Astani, C. Grätzel, S. M. Zakeeruddin, U. Röthlisberger, M. Grätzel, *Energy Environ. Sci.* **2016**, *9*, 656–662; b) Z. Li, M. Yang, J. S. Park, S. H. Wei, J. J. Berry, K. Zhu, *Chem. Mater.* **2016**, *28*, 284–292; c) J. W. Lee, S. Tan, S. Il Seok, Y. Yang, N. G. Park, *Science* **2022**, *375*, eabj1186.
[12] R. G. Niemann, L. Gouda, J. Hu, S. Tirosh, R. Gottesman, P. J. Cameron, A. Zaban, *J. Mater. Chem. A* **2016**, *4*, 17819–17827.
[13] X. Zhu, D. Yang, R. Yang, B. Yang, Z. Yang, X. Ren, J. Zhang, J. Niu, J. Feng, S. Liu, *Nanoscale* **2017**, *9*, 12316–12323.
[14] J. J. Gallardo, E. Blanco, A. Sánchez-Coronilla, J. C. Pinero, J. Navas, *Appl. Mater. Today* **2020**, *18*, 100488.
[15] M. Suri, A. Hazarika, B. W. Larson, Q. Zhao, M. Vallés-Pelarda, T. D. Siegler, M. K. Abney, A. J. Ferguson, B. A. Korgel, J. M. Luther, *ACS Energy Lett.* **2019**, *4*, 1954–1960.
[16] M. Hao, Y. Bai, S. Zeiske, L. Ren, J. Liu, Y. Yuan, N. Zarrabi, N. Cheng, M. Ghasemi, P. Chen, M. Lyu, D. He, J. H. Yun, Y. Du, Y. Wang, S. Ding, A. Armin, P. Meredith, G. Liu, H. M. Cheng, L. Wang, *Nat. Energy* **2020**, *5*, 79–88.
[17] J. M. Azpiroz, E. Mosconi, J. Bisquert, F. De Angelis, *Energy Environ. Sci.* **2015**, *8*, 2118–2127.
[18] C. Otero-Martínez, M. Imran, N. J. Schrenker, J. Ye, K. Ji, A. Rao, S. D. Stranks, R. L. Z. Hoye, S. Bals, L. Manna, J. Pérez-Juste, L. Polavarapu, *Angew. Chem. Int. Ed.* **2022**, *61*, e202205617.
[19] Q. Zhao, A. Hazarika, L. T. Schelhas, J. Liu, E. A. Gaulding, G. Li, M. Zhang, M. F. Toney, P. C. Sercel, J. M. Luther, *ACS Energy Lett.* **2020**, *5*, 238–247.
[20] M. Saliba, T. Matsui, J. Y. Seo, K. Domanski, J. P. Correa-Baena, M. K. Nazeeruddin, S. M. Zakeeruddin, W. Tress, A. Abate, A. Hagfeldt, M. Grätzel, *Energy Environ. Sci.* **2016**, *9*, 1989–1997.
[21] Y. Zhang, T. D. Siegler, C. J. Thomas, M. K. Abney, T. Shah, A. De Gorostiza, R. M. Greene, B. A. Korgel, *Chem. Mater.* **2020**, *32*, 5410–5423.
[22] D. W. Houck, B. A. Korgel, *Chem. Mater.* **2018**, *30*, 8359–8367.
[23] J. De Roo, M. Ibáñez, P. Geiregat, G. Nedelcu, W. Walravens, J. Maes, J. C. Martins, I. Van Driessche, M. V. Kovalenko, Z. Hens, *ACS Nano* **2016**, *10*, 2071–2081.
[24] V. K. Ravi, P. K. Santra, N. Joshi, J. Chugh, S. K. Singh, H. Rensmo, P. Ghosh, A. Nag, *J. Phys. Chem. Lett.* **2017**, *8*, 4988–4994.
[25] Y. Zhang, T. Shah, F. L. Deepak, B. A. Korgel, *Chem. Mater.* **2019**, *31*, 7962–7969.
[26] a) V. K. Ravi, R. A. Scheidt, A. Nag, M. Kuno, P. V. Kamat, *ACS Energy Lett.* **2018**, *3*, 1049–1055; b) E. Scharf, F. Krieg, O. Elimelech, M. Oded, A. Levi, D. N. Dirin, M. V. Kovalenko, U. Banin, *Nano Lett.* **2022**, *22*, 4340–4346.
[27] a) D. T. Moore, H. Sai, K. W. Tan, D. M. Smilgies, W. Zhang, H. J. Snaith, U. Wiesner, L. A. Estroff, *J. Am. Chem. Soc.* **2015**, *137*, 2350–2358; b) V. L. Pool, B. Dou, D. G. Van Campen, T. R. Klein-Stockert, F. S. Barnes, S. E. Shaheen, M. I. Ahmad, M. F. A. M. van Hest, M. F. Toney, *Nat. Commun.* **2017**, *8*, 14075.
[28] a) M. Avrami, *J. Chem. Phys.* **1939**, *7*, 1103–1112; b) M. Avrami, *J. Chem. Phys.* **1940**, *8*, 212–224.
[29] A. Khawam, D. R. Flanagan, *J. Phys. Chem. B* **2006**, *110*, 17315–17328.
[30] M. L. Holekevi Chandrappa, Z. Zhu, D. P. Fenning, S. P. Ong, *Chem. Mater.* **2021**, *33*, 4672–4678.
[31] W. Travis, E. N. K. Glover, H. Bronstein, D. O. Scanlon, R. G. Palgrave, *Chem. Sci.* **2016**, *7*, 4548–4556.
[32] A. Binek, F. C. Hanusch, P. Docampo, T. Bein, *J. Phys. Chem. Lett.* **2015**, *6*, 1249–1253.
[33] A. Dualeh, P. Gao, S. Il Seok, M. K. Nazeeruddin, M. Grätzel, *Chem. Mater.* **2014**, *26*, 6160–6164.
[34] E. J. Juarez-Perez, Z. Hawash, S. R. Raga, L. K. Ono, Y. Qi, *Energy Environ. Sci.* **2016**, *9*, 3406–3410.
[35] J. A. McLeod, L. Liu, *J. Phys. Chem. Lett.* **2018**, *9*, 2411–2417.
[36] D. B. Straus, S. Guo, R. J. Cava, *J. Am. Chem. Soc.* **2019**, *141*, 11435–11439.
[37] B. Zhao, S. F. Jin, S. Huang, N. Liu, J. Y. Ma, D. J. Xue, Q. Han, J. Ding, Q. Q. Ge, Y. Feng, J. S. Hu, *J. Am. Chem. Soc.* **2018**, *140*, 11716–11725.
[38] J. A. Vigil, A. Hazarika, J. M. Luther, M. F. Toney, *ACS Energy Lett.* **2020**, *5*, 2475–2482.

Manuscript received: April 28, 2023
Accepted manuscript online: June 5, 2023
Version of record online: June 26, 2023